

# Environmental Science Nano

Accepted Manuscript

This article can be cited before page numbers have been issued, to do this please use: B. Ryu, W. Zhuang, H. Jang, Z. Gao, Y. Wang and J. Chen, *Environ. Sci.: Nano*, 2025, DOI: 10.1039/D4EN00884G.



This is an Accepted Manuscript, which has been through the Royal Society of Chemistry peer review process and has been accepted for publication.

Accepted Manuscripts are published online shortly after acceptance, before technical editing, formatting and proof reading. Using this free service, authors can make their results available to the community, in citable form, before we publish the edited article. We will replace this Accepted Manuscript with the edited and formatted Advance Article as soon as it is available.

You can find more information about Accepted Manuscripts in the [Information for Authors](#).

Please note that technical editing may introduce minor changes to the text and/or graphics, which may alter content. The journal's standard [Terms & Conditions](#) and the [Ethical guidelines](#) still apply. In no event shall the Royal Society of Chemistry be held responsible for any errors or omissions in this Accepted Manuscript or any consequences arising from the use of any information it contains.

## Environmental Significance Statement

Environmental exposure to  $\text{Pb}^{2+}$  poses significant risks to humans and ecosystems, underscoring the need for a rapid and sensitive detection system for trace concentrations of  $\text{Pb}^{2+}$ . Traditional methods for  $\text{Pb}^{2+}$  detection are often costly, complicated, and time-consuming, and thus are insufficient for real-time, in situ monitoring. In this study, we present a fully portable sensor system based on the field-effect transistor (FET) technology that enables rapid, sensitive, and real-time detection of  $\text{Pb}^{2+}$ . The sensor exhibits an ultra-low detection limit of 1 nM (~0.2 ppb) and features a graphene-ink-based gate electrode that can be recycled for repeated tests. This electronic sensing advancement is significant for water quality testing and offers substantial benefits for environmental monitoring.

Environmental Science: Nano Accepted Manuscript

1  
2  
3  
4  
5  
6  
7  
8  
9  
10  
11  
12  
13  
14  
15  
16  
17  
18  
19  
20  
21  
22  
23  
24  
25  
26  
27  
28  
29  
30  
31  
32  
33  
34  
35  
36  
37  
38  
39  
40  
41  
42  
43  
44  
45  
46  
47  
48  
49  
50  
51  
52  
53  
54  
55  
56  
57  
58  
59  
60

Downloaded on 29/12/2024 05:48:36  
This article is licensed under a Creative Commons Attribution 3.0 Unported Licence.  


# A Portable and Reusable Sensor System Based on Graphene for Real-Time and Sensitive Detection of Lead Ions in Water

Byunghoon Ryu<sup>1,2,+</sup>, Wen Zhuang<sup>1,3,+</sup>, Hyun-June Jang<sup>1,3</sup>, Zhenwei Gao<sup>1,3</sup>, Yuqin Wang<sup>1,3</sup>, and Junhong Chen<sup>1,3,\*</sup>

<sup>1</sup>Chemical Sciences and Engineering Division, Physical Sciences and Engineering Directorate, Argonne National Laboratory, Lemont, Illinois 60439, USA.

<sup>2</sup>Department of Mechanical Engineering, Inha University, Incheon, 22212, Republic of Korea.

<sup>3</sup>Pritzker School of Molecular Engineering, University of Chicago, Chicago, Illinois 60637, USA.

\*Contact Email: [junhongchen@anl.gov](mailto:junhongchen@anl.gov), [junhongchen@uchicago.edu](mailto:junhongchen@uchicago.edu)

## Keywords

Pb<sup>2+</sup> detection, Portable sensor, Remote-gate field-effect transistor (RGFET), Real-time monitoring, Graphene film, Smartphone application.

1  
2  
3  
4  
5  
6  
7  
8  
9  
10  
11  
12  
13  
14  
15  
16  
17  
18  
19  
20  
21  
22  
23  
24  
25  
26  
27  
28  
29  
30  
31  
32  
33  
34  
35  
36  
37  
38  
39  
40  
41  
42  
43  
44  
45  
46  
47  
48  
49  
50  
51  
52  
53  
54  
55  
56  
57  
58  
59  
60

Downloaded on 29/12/2024 05:48:36  
This article is licensed under a Creative Commons Attribution 3.0 Unported Licence.  


## Abstract

Long-term exposure to  $\text{Pb}^{2+}$  can cause irreversible damage to the nervous, cardiovascular, and reproductive systems. Therefore, developing a fast and sensitive detection system capable of monitoring minuscule concentrations of  $\text{Pb}^{2+}$  is essential. In this study, we have demonstrated a fully portable sensor system enabling rapid, sensitive, and real-time monitoring of  $\text{Pb}^{2+}$ . The sensor system adopts the remote-gate field-effect transistor (RGFET) detection scheme and is easy to operate, even for non-experts. The sensor system comprises two printed circuit boards (PCBs): a sensor PCB with a remote gate electrode and an analyzer PCB with a metal–oxide–semiconductor field-effect transistor (MOSFET) transducer and peripheral electronics to manage sensor signals. To achieve a high sensitivity for  $\text{Pb}^{2+}$ , we utilized a graphene ink drop-casted on the sensor PCB as a sensing membrane. The graphene film is straightforward to deposit and remove, enabling the sensor PCB to be reused multiple times. The sensor system is further linked to a smartphone app that instantly monitors the sensor response, allowing for rapid point-of-use detection. The sensor has a high sensitivity of 21.7% when the limit of detection (LOD) value of 1 nM ( $\sim 0.2$  ppb) is being detected, and the typical detection time for each sample is approximately 60 seconds. This portable sensor system advances sensing technologies and could potentially supplement expensive, laborious conventional sensing equipment.

## 1. Introduction

The U.S. Environmental Protection Agency (EPA) defines the maximum contaminant level (MCL) of lead ions ( $\text{Pb}^{2+}$ ) in drinking water as 15 ppb [1]. However, there is no safe level of lead in drinking water because prolonged exposure to  $\text{Pb}^{2+}$  can accumulate in the human body over time, which results in critical impairment to the nervous, cardiovascular, and reproductive systems [2, 3]. Therefore, developing a detection system that can monitor the minuscule  $\text{Pb}^{2+}$  in water rapidly and sensitively is imperative, enabling diagnostic and restorative measures to prevent long-term damages. However, current prevailing methods such as inductively coupled plasma mass spectrometry (ICP-MS) [4], atomic fluorescence spectroscopy [5], and atomic absorption spectroscopy [6] cannot meet these requirements as they need expensive instruments with operational experts and time-consuming sample delivery, which prevents timely monitoring of toxic  $\text{Pb}^{2+}$ .

To tackle the above-mentioned challenges, several attempts to develop portable sensors facilitating rapid and sensitive detection of  $\text{Pb}^{2+}$  have been reported [7-11]. Stephanie et al. [10] developed a handheld microfiber-based sensor detecting optical signal changes related to the concentration of  $\text{Pb}^{2+}$  around the microfiber. Particularly, the surface of the fiber was functionalized with L-glutathione (GSH) receptors altering the effective refractive index upon binding with  $\text{Pb}^{2+}$ , which results in the red shift of the output transmission spectrum of incident light traveling through the fiber. The limit of detection (LOD) of this sensor was  $\sim 5$  ppb, and the typical detection time was  $\sim 4$  min for each pre-prepared sample. Yaying et al. [7] adopted a commercial electronic balance as a readout device precisely measuring the weight of the overflowed water associated with the concentration of  $\text{Pb}^{2+}$ . More specifically, the activation of DNAzyme occurred in the presence of  $\text{Pb}^{2+}$ , which releases hybridized platinum nanoparticles

(PtNPs), subsequently provoking the catalytic reaction with hydrogen peroxide ( $H_2O_2$ ) in a sealed glass bottle equipped with a drainage tube. Therefore, the water drained out of the tube because the pressure in the sealed bottle increased due to the formation of oxygen gas. This detection approach took  $\sim 60$  min for each detection cycle, and the LOD was  $\sim 0.83$  nM ( $\sim 0.17$  ppb). Similarly, Chao et al. [8] employed DNAzyme to build a portable detection scheme for  $Pb^{2+}$ . In this scheme, the DNAzyme detained a crosslinker substrate for the hydrogel, releasing the substrate once  $Pb^{2+}$  exists, which induces the phase transition of hydrogel from gel to a solution. Eventually, the solution phase of hydrogel climbed into a capillary channel, whose height was measured as a sensor response. The detection time and LOD were  $\sim 1$  h and 10 nM ( $\sim 2$  ppb), respectively. Despite such encouraging progress in developing portable  $Pb^{2+}$  sensors, there remain unmet technical voids because they are either still hard to operate for the novice or not fully portable, requiring additional analyzers.

Meanwhile, field-effect transistor (FET) sensors have been extensively studied for lead ion detection [12-15], owing to their distinct advantages in rapid response, ultralow detection limits and direct digital readouts. Among these FET sensors, remote-gate (extended-gate) FET devices have emerged as promising candidates due to their enhanced operational stability [16-19], which benefits from the structural isolation of the semiconductor channel of the FET from the solution-contacting sensing area. Despite their impressive performance, critical challenges remain in manufacture scalability, device reusability and circuit integration, which may limit their practical applications in portable systems.

Here we report a fully portable sensor system enabling rapid, sensitive, and real-time monitoring for  $Pb^{2+}$  as well as easy to operate even for a layperson, based upon the remote-gate field-effect transistor (RGFET) detection scheme known for high detection stability and reliability [18, 19].

The portable sensor consists of a sensor printed circuit board (PCB) and an analyzer PCB corresponding to a remote gate and a n-type metal-oxide-semiconductor field-effect transistor (MOSFET) transducer of the RGFET, respectively. In particular, we make use of graphene ink drop-casted on top of the sensor PCB as a sensing membrane, achieving high sensitivity toward  $\text{Pb}^{2+}$  due to the high surface-to-volume ratio and electrical conductivity of the graphene nanoflakes [20, 21]. Furthermore, the Cu-plated surface of the sensor PCB provides adequate adhesion to the graphene ink, allowing facile deposition and removal, which results in the ability to reuse the sensor PCB repeatedly. Interfacing with a smartphone application instantaneously visualizing the sensor response, the portable sensor system exhibits a high sensitivity of 21.7 % when detecting its LOD value of 1 nM ( $\sim 0.2$  ppb), and the typical detection time for each sample is 60 sec. Such a portable sensor could be further developed into a reliable detection system supplementing expensive and labor-intensive conventional sensing instruments.

## 2. Experimental method

### 2.1. Design the analyzer PCB of the portable sensor system

First, a 32-bit microcontroller (MCU, Seeed Xiao) was chosen to control peripheral electronics manipulating and transmitting sensor signals. To generate and supply a precisely adjusted reference voltage (2.054 V) to a reference electrode (BASi, MW-2021), a shunt voltage reference (LM4040) was integrated into the analyzer PCB. When the surface potential was delivered from the sensor PCB to the gate pin of the MOSFET (CD4007), the drain current flew into a resistor connected to the drain pin of the n-type MOSFET, which converted the drain current to voltage-type sensor signals. Such sensor signals traveled to a 16-bit analog-to-digital chip (AD1115), then

were digitized, enabling a readout from the MCU. The sensor signals were further delivered to a mobile app through a Bluetooth module (HM-10) or displayed on an OLED panel.

## 2.2. Functionalize the sensor PCB of the portable sensor system

Before functionalization, graphene ink (Sigma-Aldrich, 793663, 2.4 wt. % graphene nanoflakes) was diluted with the background solvent consisting of 85% cyclohexanone (Sigma-Aldrich, 398241) and 15% terpineol (Sigma-Aldrich, 86480). The as-prepared graphene ink was deposited onto the Cu-plated electrode pad of the sensor PCB via drop casting and post-annealed using a horizontal furnace for 30 min under an argon gas environment at 250 °C. Then, 1-pyrene butyric acid (PBA) (TCI, P1213) was dissolved in dimethylformamide (DMF) (Sigma-Aldrich, 319937) to prepare 10 mM solution. Next, a droplet (3  $\mu\text{L}$ ) of the PBA solution was pipetted onto the graphene film and incubated in a closed chamber for 1.5 h. The functionalized graphene film was washed with DMF for three times to remove unbounded PBA and dried with nitrogen gas for sensor measurements.

## 2.3 Sensor measurement and operation

The  $\text{Pb}^{2+}$  solutions were prepared by dissolving  $\text{PbCl}_2$  powder (Sigma-Aldrich, 268690) in deionized water or tap water, and diluted to targeted concentrations. For selectivity tests, the interference solutions were prepared similarly with  $\text{CuCl}_2$  (Sigma-Aldrich, 459097),  $\text{ZnCl}_2$  (Sigma-Aldrich, 429430),  $\text{FeCl}_3$  (Sigma-Aldrich, 157740),  $\text{NiCl}_2$  (Sigma-Aldrich, 654507),  $\text{MnCl}_2$  (Sigma-Aldrich, 244589),  $\text{CaCl}_2$  (Sigma-Aldrich, 223506),  $\text{MgCl}_2$  (Sigma-Aldrich, 255777), &  $\text{NaCl}$  (Sigma-Aldrich, S7653), respectively. A 15  $\mu\text{L}$  testing solution prepared above was pipetted onto the sensor PCB. An Ag/AgCl reference electrode contacted the testing solution in order to apply the gate bias for all measurements. An n-type MOSFET (CD4007) was connected with the

1  
2  
3  
4  
5  
6  
7  
8  
9  
10  
11  
12  
13  
14  
15  
16  
17  
18  
19  
20  
21  
22  
23  
24  
25  
26  
27  
28  
29  
30  
31  
32  
33  
34  
35  
36  
37  
38  
39  
40  
41  
42  
43  
44  
45  
46  
47  
48  
49  
50  
51  
52  
53  
54  
55  
56  
57  
58  
59  
60



1  
2  
3 sensor PCB as a transducer and used for all measurements consistently. All the transfer curves  
4 were measured by a Keithley 4200A semiconductor analyzer with a drain voltage set at 50 mV.  
5  
6 Each testing solution was then removed by pipetting after each round of measurement. The  
7  
8 threshold voltage was calculated as the gate voltage corresponding to drain current of 1  $\mu$ A in each  
9  
10 transfer curve and the average signal changes were calculated based on the results from three  
11  
12 measurements. The smartphone application was designed using Android Studio. Each detection  
13  
14 curve, after finishing measurement, was extracted in an ASCII format and sent to email or  
15  
16 messenger apps.

### 3. Results and discussion

#### 3.1. Strategies to design a portable RGFET sensor

RGFET offers plenty of benefits in sensing applications, such as fast response, high sensitivity,  
and detection stability [18, 19]. Especially the stability is a favorable characteristic hard to expect  
from numerous other nano-sensors, making the RGFET likely to be further developed into a  
miniaturized, portable and commercial sensor. Such stability of the RGFET is attributed to its  
device structure formulated by the equation below [16].

$$V_{th} = V_{th\_FET} + E_{ref} + \phi_{lj} - \phi_s + \chi_{sol} + \frac{\phi_G}{q} \quad (1)$$

where  $V_{th}$  and  $V_{th\_FET}$  are threshold voltages of the RGFET and its component, MOSFET,  
respectively,  $E_{ref}$  is the standard potential of an Ag/AgCl reference electrode (+0.209 V vs. NHE,  
BASi Corp.),  $\phi_{lj}$ ,  $\phi_s$ , and  $\chi_{sol}$  are potentials associated with the liquid junction, sensing  
membrane, and solution interfaces, and  $\phi_G$  is the work function of the graphene. According to  
Equation 1, the change in threshold voltage of the RGFET,  $V_{th}$ , only depends on events at the



1  
2  
3 surface of the sensing membrane because  $V_{th\_FET}$  and  $E_{ref}$  are stable variables derived from a  
4 commercial MOSFET and the reference electrode, respectively. Therefore, the RGFET exhibits  
5 high detection stability when it operates with the optimized sensing membrane and protocols.  
6  
7  
8  
9

10 **Figure 1** schematically shows the graphene RGFET consisting of a remote gate and a MOSFET,  
11 which requires a bulky device setup for the detection test. In conventional operation, transfer  
12 characteristic curves of the RGFET are measured repeatedly by a skilled operator as various  
13 concentrations of analytes are introduced to the sensing membrane. Subsequently, additional post-  
14 processes need to be done to accurately extract the sensor responses,  $\Delta V_{th}$ , associated with the  
15 concentration of the analytes, which is time-consuming and far from real-time detection, as shown  
16 in **Figure 1 (c)**. To achieve facile and real-time detection capability, it is more reasonable to  
17 capture another sensor response of the RGFET,  $I_{DS}$ , continuously and directly correlate those with  
18 the concentrations of analytes, as shown in **Figure 1 (d)**.  $\Delta V_{th}$  and  $\Delta I_{ds}$  are both derived features  
19 from the shifts of FET transfer curves, while  $\Delta I_{ds}$  signals are amplified by the field effect and  
20 more accessible for circuit integration. Along with such a modified sensor operation approach, the  
21 RGFET, including a bulky and expensive analyzer, necessarily be miniaturized to develop a  
22 portable sensor. Specifically, the remote gate shown in **Figure 1 (a)** and the MOSFET and analyzer  
23 shown in **Figure 1 (b)** are preferably designed into a sensor PCB and an analyzer PCB,  
24 respectively. Considering these strategies, it is feasible to reduce the size of the conventional  
25 RGFET sensor and make it portable, while exhibiting high sensitivity, stability, and real-time  
26 monitoring capability.  
27  
28  
29  
30  
31  
32  
33  
34  
35  
36  
37  
38  
39  
40  
41  
42  
43  
44  
45  
46  
47  
48  
49  
50  
51  
52  
53  
54  
55  
56  
57  
58  
59  
60

### 3.2. The sensor PCB design and deposition of graphene

As a first step, the remote gate of the RGFET is replaced with the sensor PCB shown in **Figure 2 (a)**. The sensor PCB has a miniaturized size of 38 mm × 18 mm, consisting of a circular electrode pad, which is a substrate for the graphene sensing membrane, and a USB connector prepared for facile connection with the analyzer PCB. The diameter of the exposed pad is designed to be 5 mm, which makes it more convenient to deposit the graphene film since the whole region of the pad is easily covered by drop-casting of a single droplet of graphene ink (1.5 μL). **Figure 2 (b)** shows graphene films deposited on the pad using various concentrations of ink to optimize the thickness of the graphene. A commercially available graphene ink was purchased from Sigma-Aldrich (Product No. 793663) and sequentially diluted three times in each step by adding its background solvent (cyclohexanone/terpineol). Initially, all four graphene ink droplets occupy the entire pad surface but eventually result in different coverages of graphene films after drying and annealing. Specifically, the graphene ink diluted three times produces a full-coverage film while further diluted inks led to low-coverage films. The thickness of the graphene films is evaluated via cross-sectional Scanning Electron Microscopy (SEM) (**Figure S1**), and **Figure 2 (c)** shows thickness profiles obtained from the full coverage films formed using pristine and 3× diluted inks. The thickness of film produced using the 3× diluted ink is ~ 0.91 μm, which is ~ 76% thinner than that produced using the pristine ink (~ 3.89 μm). It should be noted that thin graphene film is beneficial because the thinner film is prone to form stable interfacial contact with the electrode pad. Therefore, the thinner one out of two full coverage graphene films were chosen for the sensing membrane of the portable sensor. **Figure 2 (d)** displays a scanning electron microscopy (SEM) image of the thin graphene film. Graphene nanoflakes are evenly stacked, completely covering the electrode pad with no vacant areas. Lastly, **Figure 2 (e)** compares the resistivity of the film before and after the

annealing process. The commercial graphene ink used in this study contains ethyl cellulose as a dispersant, degrading the graphene film's electrical conductivity but is removable under high temperatures of around  $\sim 300$  °C. After annealing, the resistivity of the graphene film is significantly reduced to  $\sim 220$  m $\Omega$ ·cm. Such a low resistivity of the film is in good agreement with previously reported values, which proves its capability of being a suitable sensing membrane [22].

### 3.3. Pb<sup>2+</sup> detection using the sensor PCB with graphene films

To verify the detection capability toward Pb<sup>2+</sup>, two sensor PCBs with deposited graphene films using pristine and 3 $\times$  diluted inks are prepared, as shown in **Figure 3 (a)**. Here, the sensor PCB holding a thin graphene film is distinctively noticeable because the reddish color pattern on the film originates from the thin-film interference. Before the detection test, both sensor PCBs are functionalized using 1-pyrenebutyric acid (PBA) conjugated with graphene nanoflakes via  $\pi - \pi$  interactions, as depicted in **Figure 3 (b)**. **Figure S2** shows the contact angle profiles of the prepared thin films and reveals that the surface hydrophilicity significantly increases after surface functionalization, suggesting a successful conjugation of PBA probes on the graphene surface. The PBA is responsible for the sensitive and selective detection of Pb<sup>2+</sup> because it bears the carboxylic acid end group, which provokes a chelation reaction with Pb<sup>2+</sup> ions, resulting in lead carboxylates [23]. Chelation significantly changes the electric double-layer (EDL) and thus alters the surface potential of the electrode [24], which leads to the shift of the FET transfer curve. As the concentration of lead ions increases, the shift of the transfer curve increases until reaching the saturation point. It is worth noting that graphene films on the sensor PCBs remained intact despite prolonged exposure to an aqueous environment during the functionalization process. This is attributed to the relatively rough surface of the Cu-plated electrode pad, as shown in **Figure S3**,

1  
2  
3  
4  
5  
6  
7  
8  
9  
10  
11  
12  
13  
14  
15  
16  
17  
18  
19  
20  
21  
22  
23  
24  
25  
26  
27  
28  
29  
30  
31  
32  
33  
34  
35  
36  
37  
38  
39  
40  
41  
42  
43  
44  
45  
46  
47  
48  
49  
50  
51  
52  
53  
54  
55  
56  
57  
58  
59  
60

Open Access Article. Published on 29 July 2024. Downloaded on 2/26/2024 4:05:48 AM.  
This article is licensed under a Creative Commons Attribution 3.0 Unported Licence.



1  
2  
3  
4  
5  
6  
7  
8  
9  
10  
11  
12  
13  
14  
15  
16  
17  
18  
19  
20  
21  
22  
23  
24  
25  
26  
27  
28  
29  
30  
31  
32  
33  
34  
35  
36  
37  
38  
39  
40  
41  
42  
43  
44  
45  
46  
47  
48  
49  
50  
51  
52  
53  
54  
55  
56  
57  
58  
59  
60

which provides sufficient adhesion to prevent the films from delaminating. **Figure 3 (c)** shows the detection setup for  $\text{Pb}^{2+}$ , including a commercial MOSFET (CD4007), an Ag/AgCl reference electrode (MW-2021), and a semiconductor analyzer. The reference electrode is in contact with a water solution containing  $\text{Pb}^{2+}$ , which supplies the sweeping voltage to the sensor PCB. Afterward, altered surface potential owing to the binding reactions is transmitted to the gate of the MOSFET, which modulates its transfer characteristics. **Figure 3 (d)** plots transfer characteristic curves shifting with respect to the concentration of  $\text{Pb}^{2+}$ , measured using the sensor PCB with a thin graphene film. As a comparison, a plot of transfer curves obtained using the sensor PCB with a thick graphene film is shown in **Figure S4**. Each transfer curve is acquired after 5 min incubation per  $\text{Pb}^{2+}$  solution droplet. Subsequently, the threshold voltage,  $V_{th}$ , of each curve is captured by investigating intersects when extending the horizontal line at  $I_{DS} = 1 \mu\text{A}$  and serves as a sensor response (R). With the increasing concentration of  $\text{Pb}^{2+}$ , threshold voltages increased accordingly, attributed to the formation of lead carboxylates which repel electrons and deplete the semiconductor channel of the n-type MOSFET [25, 26]. **Figure 3 (e)** compares the change in threshold voltage vs.  $\text{Pb}^{2+}$  concentrations using two sensor PCBs composed of thick and thin graphene films. The sensor responses,  $V_{th}$ , obtained from both sensor PCBs are directly proportional to the concentrations, which demonstrates the sensor's ability to detect  $\text{Pb}^{2+}$ . The sensitivity of the sensor, defined as the relative change in sensor responses  $((R_i - R_0)/R_0 \times 100 \%)$ , is further calculated and displayed in **Figure 3 (f)**. The sensitivity toward  $\text{Pb}^{2+}$  detection using the sensor PCB with the thin graphene film is about 10-fold higher than that of the sensor PCB with the thick graphene film, attributed to the fact that the thin graphene film could form a more stable electrical connection to the electrode pad, which results in effective transfer of the surface potential

change to the MOSFET [27]. As a result of these comparative tests, it was decided to use a thin layer of graphene as a sensitive sensing membrane to develop the portable sensor.

### 3.4. Selectivity and reusability of the sensor PCB

The selectivity and reusability of the sensor PCB containing the thin graphene film were additionally evaluated. **Figure 4 (a)** shows the sensitivity of the sensor toward major interfering cations in municipal water at a concentration of 100 nM (*i.e.*, 20 ppb). Notably,  $\text{Pb}^{2+}$  elicits the most pronounced response, with a sensitivity approximately ten-fold greater than that of the other ions, which underscores the sensor's selectivity toward  $\text{Pb}^{2+}$ . The selectivity is likely attributed to the nature that lead ions have much stronger affinity toward carboxylic groups to form complexation compared to other cations [28]. An important advantage of the sensor PCB worth highlighting is its ability to be reused multiple times. Specifically, the graphene film deposited on the sensor PCB can be readily eliminated once finishing its detection through a straightforward wiping process using an alcohol wipe as shown in **Figure S5**. Subsequently, the sensor PCB can be refreshed for the following assay via drop-casting of fresh graphene ink. **Figure 4 (b)** describes the refreshing process and the reusability of the sensor PCB. To demonstrate the reusability, detection tests for  $\text{Pb}^{2+}$  were repeatedly conducted while the sensor PCB was refreshed three times. The sensor response plot in **Figure 4 (b)** indicates no significant degradation in the threshold voltages for every  $\text{Pb}^{2+}$  concentration, despite the sensor PCB being repeatedly used, confirming its reusability.

### 3.5. Design of the fully portable sensor system

**Figure 5 (a)** shows the schematic design of an analyzer PCB capable of substituting the bulky and expensive commercial analyzer to be assembled with the sensor PCB to construct the portable sensor system. The analyzer PCB consists of a series of electrical components, including an operational amplifier, a 16-bit analog-to-digital converter, and a Bluetooth module for amplifying, digitizing, and transferring sensor signals, respectively. Particularly, the footprint of the PCB is 43 mm × 30 mm, powered by a tiny 3.7 V LiPo battery, which guarantees its excellent portability. A detailed circuit diagram of the analyzer PCB is presented in **Figure S6**. In operation, the analyzer PCB delivers precisely regulated voltage to the sensor PCB via the reference electrode, resulting in the drain current ( $I_{DS}$ ) of the MOSFET. **Figure S7** shows the drain current as a function of the gate and drain voltage for the MOSFET (CD4007). Such a time-dependent drain current associated with the concentration of  $Pb^{2+}$  is subsequently converted to the voltage, amplified, and wirelessly transmitted to a smartphone using the Bluetooth module. **Figure 5 (b)** displays the assembly of the sensor and analyzer PCBs and a prototype designed by packaging them. It is worth noting that the assembly process of PCBs can be accomplished with ease through a pair of standard USB connectors. Moreover, the overall dimensions of the prototype are 60 mm (L) × 40 mm (W) × 50 mm (H), rendering it both compact and portable. The sensor signals from the prototype can be transmitted to a smartphone application to facilitate prompt and real-time monitoring, as shown in **Figure 5 (c)**. The mobile application integrates a calibration equation to exhibit the concentrations of  $Pb^{2+}$  and plot their variation over time. Upon exceeding the EPA's MCL for  $Pb^{2+}$  in water, the application notifies the user of the potential hazard through a visible alarm.

### 3.6. $Pb^{2+}$ detection using the portable sensor

**Figure 6** evaluates the efficacy of the portable sensor system in  $\text{Pb}^{2+}$  detection. **Figure 6 (a)** presents a real-time plot showcasing the detection of various concentrations of  $\text{Pb}^{2+}$ . After switching on the sensor, there is an upsurge in sensor signals as the sample solutions are introduced after around 20 sec. A decrease in the sensor signal is observed with an increase in the concentration of  $\text{Pb}^{2+}$ , attributed to the formation of lead carboxylates, which reduces the drain current of the MOSFET. It is worth mentioning that the sensor signals attain a steady level within 60 sec of initiating measurement, enabling the sensor to detect  $\text{Pb}^{2+}$  rapidly. The sensitivity of the sensor is calculated using the sensor signals recorded at 60 sec, as illustrated in **Figure 6(b)**. The overall sensitivity of the portable sensor is noticeably high, surpassing 20 % at all concentrations. This is attributed to its working principle measuring  $I_{DS}$  that provides high response toward  $\text{Pb}^{2+}$  detection, and the signal amplification circuit integrated into the analyzer PCB. In particular, the sensor's sensitivity remains impressive, with a value of 21.7 %, when measuring a low concentration of  $\text{Pb}^{2+}$  at 1 nM (*i.e.*, 0.2 ppb), which remains high compared to the sensitivity of other portable sensors previously reported. To provide a more comprehensive comparison, we present in **Table 1** the critical characteristics of our portable sensor alongside those of other sensors utilized for  $\text{Pb}^{2+}$  detection [7-11]. **Figure S8** demonstrates further assessment of the portable sensor's ability to detect  $\text{Pb}^{2+}$  through the utilization of a sensor PCB containing a thick graphene film, leading to a much lower sensitivity.

The detection ability of the portable sensor in tap water spiked with  $\text{Pb}^{2+}$  is further assessed in **Figure 6 (c)**. To mimic the  $\text{Pb}^{2+}$ -contaminated tap water samples, test samples were prepared by spiking  $\text{PbCl}_2$  salts into lead-free tap water at varying concentrations (10, 30, 100 & 300 ppb). The portable sensor exhibited a high sensitivity in all test samples, even at the lowest concentration of 10 ppb, which is below the EPA action level/MCL (15 ppb). The calibration plot depicted in



**Figure 6 (d)** is generated by processing and fitting multiple test results. The resulting calibration equation is extracted from the plot and subsequently integrated into the portable sensor system. Consequently, such an integration allows the sensor to provide timely warnings regarding the presence of toxic  $\text{Pb}^{2+}$  levels in tap water via the mobile application.

#### 4. Conclusion

In conclusion, we have developed and presented a fully portable sensor system for the rapid, sensitive, and real-time monitoring of  $\text{Pb}^{2+}$ . The sensor is based on the RGFET detection scheme and is easy to operate, even for those without specialized training. The portable sensor consists of two PCBs: a sensor PCB with a remote gate and an analyzer PCB including a MOSFET transducer and peripheral electronics for handling sensor signals. To achieve a high sensitivity toward  $\text{Pb}^{2+}$ , graphene ink drop-casted on top of the sensor PCB is used as a sensing membrane. Such a graphene film is facile to deposit and remove, thereby allowing for the reuse of the sensor PCB multiple times. The portable sensor system is interfaced with a smartphone application that instantaneously monitors the sensor response, enabling rapid point-of-use detection. This portable sensor system can be a reliable, cost-effective supplement for expensive, labor-intensive conventional sensing instruments. Overall, the development of this portable sensor represents a significant advance in the field of sensing technologies, as it provides a fast and sensitive approach to detecting  $\text{Pb}^{2+}$  in real-time, which could ultimately benefit various practical applications, including environmental monitoring and medical diagnosis.

#### Conflicts of interest

J.C. is a founder and consultant of NanoAffix Science LLC. NanoAffix did not fund the research reported here.

### Acknowledgments


B.R. acknowledges the support from the National Research Foundation of Korea (NRF) grant funded by the Korean Government (MSIT) (RS-2023-00247462) and the INHA UNIVERSITY Research Grant. W.Z. acknowledges the support from an NRT grant from the National Science Foundation (Grant No. 2022023).

### Appendix A. Supplementary data

Supplementary data associated with this article can be found, in the online version, at

1  
2  
3  
4  
5  
6  
7  
8  
9  
10  
11  
12  
13  
14  
15  
16  
17  
18  
19  
20  
21  
22  
23  
24  
25  
26  
27  
28  
29  
30  
31  
32  
33  
34  
35  
36  
37  
38  
39  
40  
41  
42  
43  
44  
45  
46  
47  
48  
49  
50  
51  
52  
53  
54  
55  
56  
57  
58  
59  
60

This article is licensed under a Creative Commons Attribution 3.0 Unported Licence.



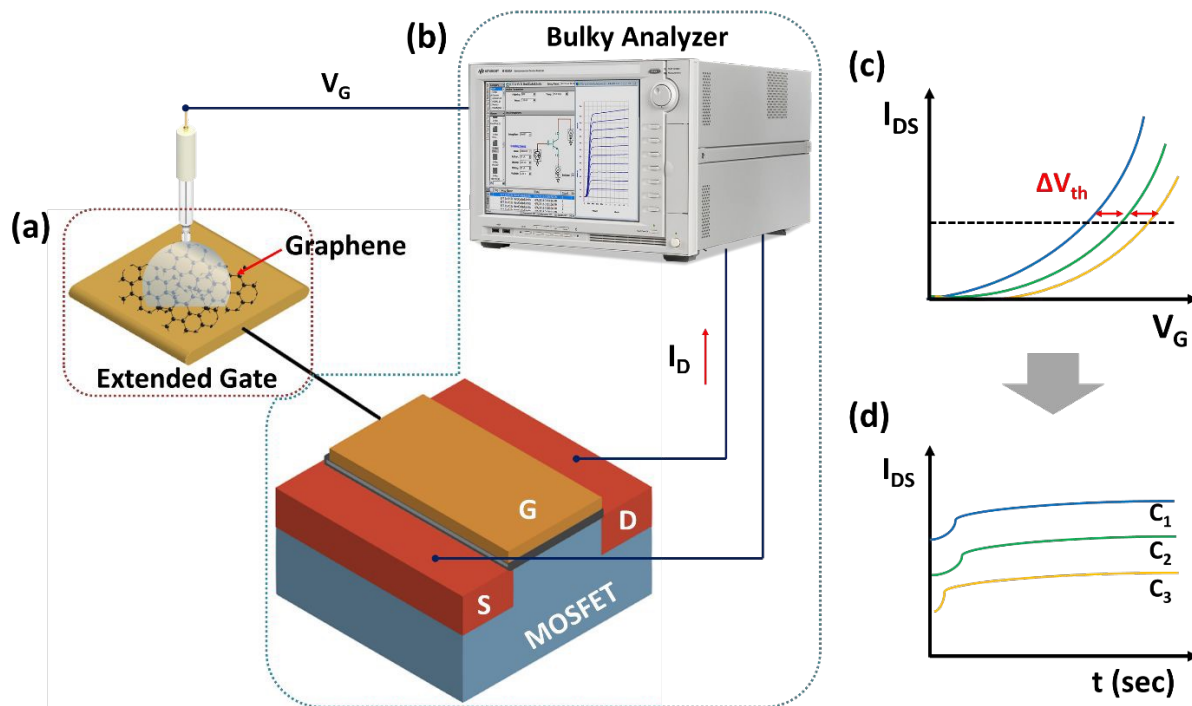


**Figure 1.** Conventional setup for operating a remote gate graphene sensor. (a) A remote gate separated from a MOSFET transducer. (b) A transducer and an analyzer for acquiring sensor signals. (c) Transfer characteristic curves observed in typical operation. (d) Real-time monitoring of  $I_{DS}$  for the portable sensor operation.

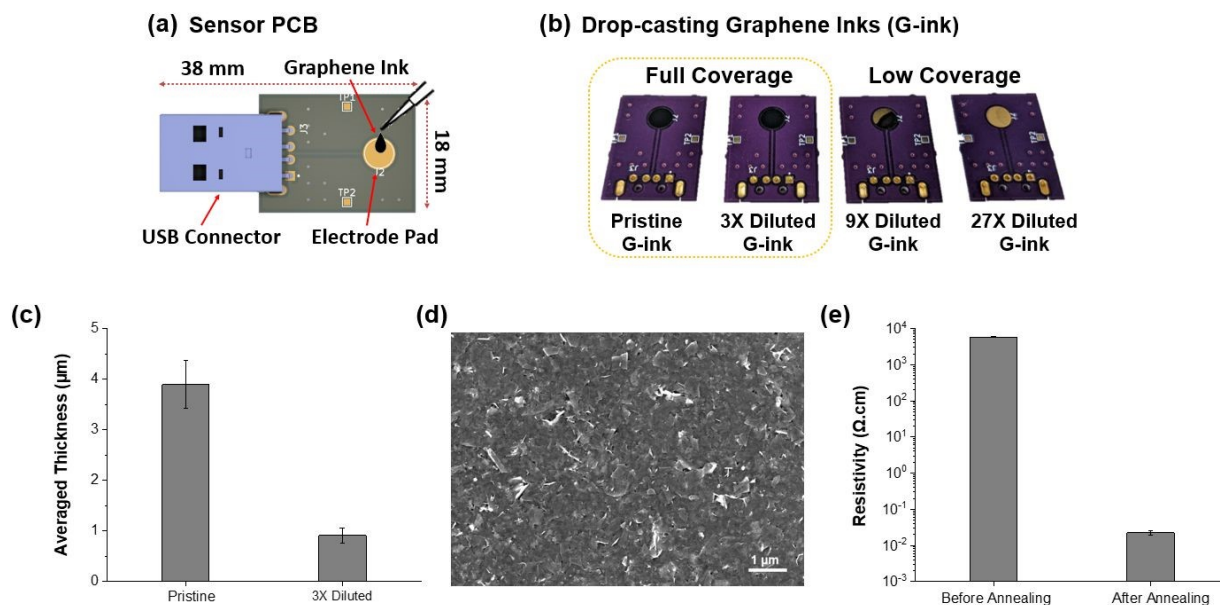


**Figure 2.** A sensor PCB replacing the conventional remote gate. (a) A schematic of the sensor PCB including a USB connector for facile connection to an analyzer PCB. (b) Optimization of graphene ink deposition onto the electrode pad. (c) Thickness profiles obtained from the films formed using pristine and 3x diluted inks. (d) An SEM image of the film deposited by using 3x diluted graphene ink. (e) Comparison of electrical resistivity of the graphene film prepared by 3x diluted ink before and after the annealing process.

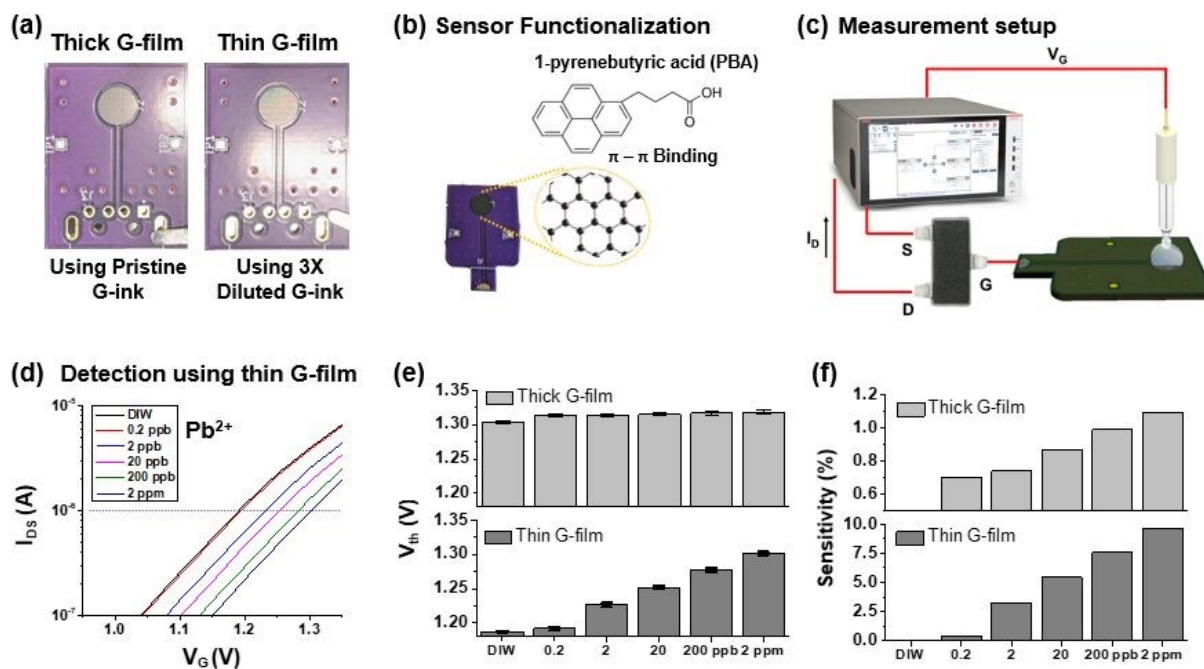


**Figure 3.** Lead ion detection using the sensor PCB drop-casted by graphene film (G-film). (a) Sensor PCBs bearing thick and thin G-films, deposited by using pristine and 3x diluted G-inks, respectively. (b) Functionalization of the sensor PCBs for lead ion detection. (c) Detection setup using the sensor PCB, MOSFET, and analyzer. (d) Transfer curves of the MOSFET upon detection of lead ions ranging from 0.2 ppb to 2 ppb using thin G-film sensor. (e) and (f) Changes in threshold voltages ( $V_{th}$ ) and sensitivity (%) with respect to lead ion concentrations using both thick and thin G-film sensors.

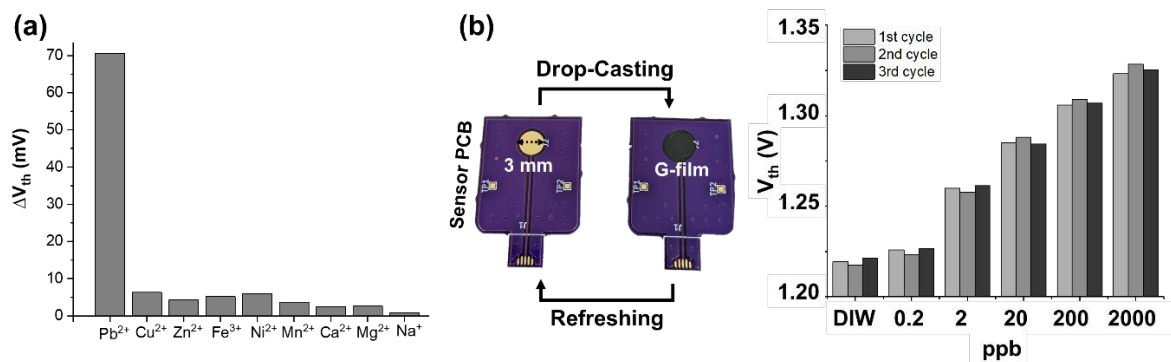


**Figure 4.** Selectivity and reusability of the graphene sensor. (a) Sensor responses toward various heavy metal ions with a concentration of 100 nM. (b) A process to refresh the sensor PCB and lead ion detection using the same graphene sensor PCB recycled three times.

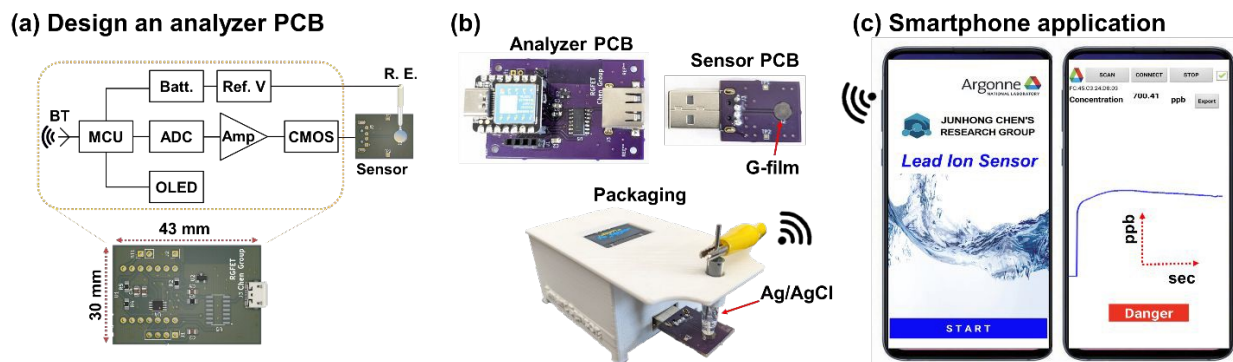


**Figure 5.** A portable sensor system for real-time monitoring of lead ions in drinking water. (a) A schematic of the analyzer PCB. (b) A prototype of the portable sensor including the analyzer and sensor PCBs. (c) A wireless communication capability of the portable sensor system with a smartphone application.

1  
2  
3  
4  
5  
6  
7  
8  
9  
10  
11  
12  
13  
14  
15  
16  
17  
18  
19  
20  
21  
22  
23  
24  
25  
26  
27  
28  
29  
30  
31  
32  
33  
34  
35  
36  
37  
38  
39  
40  
41  
42  
43  
44  
45  
46  
47  
48  
49  
50  
51  
52  
53  
54  
55  
56  
57  
58  
59  
60

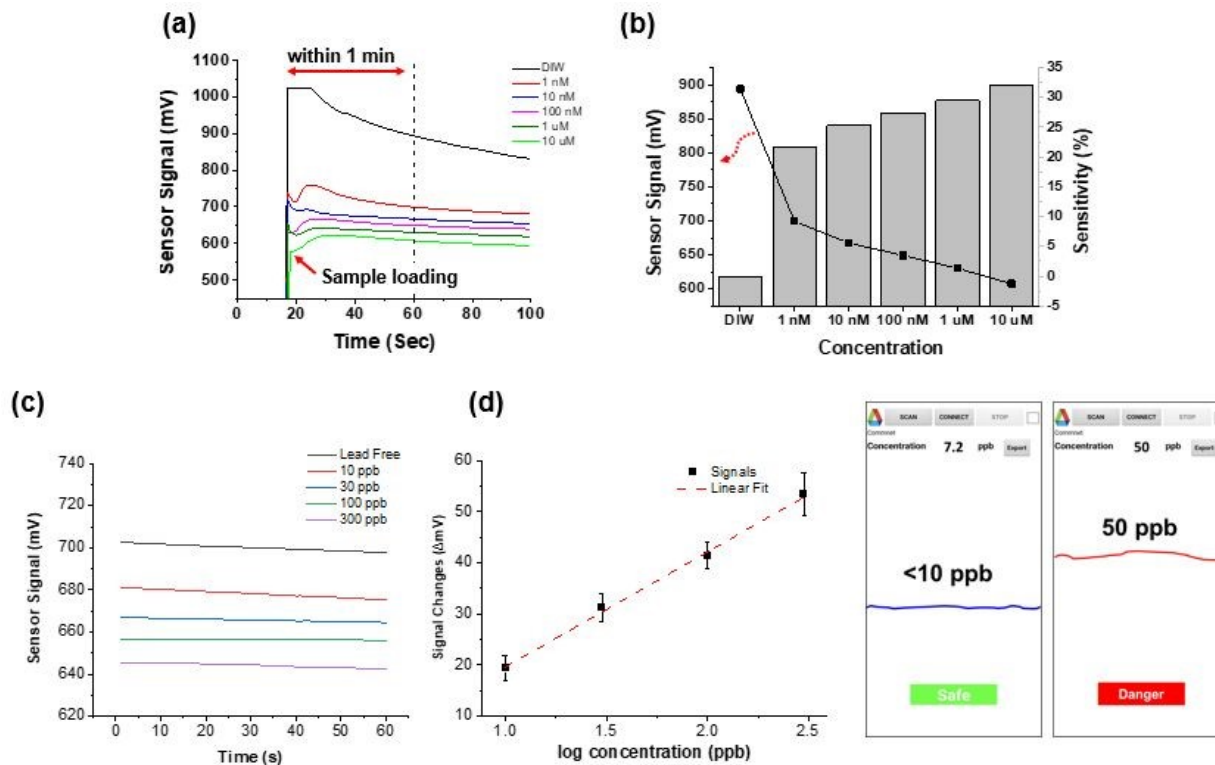


**Figure 6.** Lead ion detection using the portable sensor system. (a) A real-time detection plot as a function of lead ion concentrations. (b) Sensitivity of the portable sensor system toward the lead ion, calculated using the relative change in sensor signals captured at 60 sec from (a). (c) Real-time detection of lead ions spiked in tap water. (d) A calibration plot of the portable sensor system and the ability to warn the toxic lead ions in tap water using the smartphone application.



**Table 1.** Comparison of portable sensors for lead ion detection

| Detection method  | Sensitivity             | LOD                   | Detection Time | Note  | Reference |
|---|-------------------------|-----------------------|----------------|---|-----------|
| DNAzyme based biosensor on a portable optic fiber                 | ~ 10.3 %<br>(@ 0.2 ppb) | 0.2 ppb<br>(1.03 nM)  | 10 min         | Require a bulky fluorescent analyzer                | [11]      |
| DNAzyme based visual capillary sensor                             | ~ 1900 %<br>(@ 2 ppb)   | 2 ppb<br>(10 nM)      | 1 h            | Require a ruler to measure the capillary distance   | [8]       |
| Handheld microfiber-based sensor                                  | ~ 0.06 %<br>(@ 10 ppb)  | 5 ppb<br>(~ 24 nM)    | 4 min          | Size of the whole system<br>203 × 149 × 65 mm       | [10]      |
| DNAzyme based sensor using electronic balance as a readout device | ~ 64.8 %<br>(@ 5 ppb)   | 0.17 ppb<br>(0.83 nM) | 60 min         | Require skilled operators and an expensive balance  | [7]       |
| Ion-responsive photonic hydrogel sensor                           | ~ 4.34 %<br>(@ 100 ppm) | 200 ppb<br>(1 μM)     | 180 min        | Require a fiber optical spectrometer                | [9]       |
| Graphene on a portable RGFET sensor                               | 21.7 %<br>(@ 0.2 ppb)   | 0.2 ppb<br>(1 nM)     | 60 sec         | Small size of the whole system<br>(60 × 40 × 50 mm) | This work |

1  
2  
3  
4  
5  
6  
7  
8  
9  
10  
11  
12  
13  
14  
15  
16  
17  
18  
19  
20  
21  
22  
23  
24  
25  
26  
27  
28  
29  
30  
31  
32  
33  
34  
35  
36  
37  
38  
39  
40  
41  
42  
43  
44  
45  
46  
47  
48  
49  
50  
51  
52  
53  
54  
55  
56  
57  
58  
59  
60




## REFERENCES

- [1] US Environmental Protection Agency, Control of lead and copper, Electronic Code of Federal Regulations, 2020.
- [2] Canfield RL, Henderson Jr CR, Cory-Slechta DA, Cox C, Jusko TA, Lanphear BP. Intellectual impairment in children with blood lead concentrations below 10  $\mu\text{g}$  per deciliter. *New England journal of medicine*. 2003 Apr 17;348(16):1517-26.
- [3] Edwards M. Fetal death and reduced birth rates associated with exposure to lead-contaminated drinking water. *Environmental science & technology*. 2014 Jan 7;48(1):739-46.
- [4] Balcaen L, Bolea-Fernandez E, Resano M, Vanhaecke F. Inductively coupled plasma–Tandem mass spectrometry (ICP-MS/MS): A powerful and universal tool for the interference-free determination of (ultra) trace elements–A tutorial review. *Analytica chimica acta*. 2015 Sep 24;894:7-19.
- [5] Karadjova IB, Lampugnani L, D’Ulivo A, Onor M, Tsalev DL. Determination of lead in wine by hydride generation atomic fluorescence spectrometry in the presence of hexacyanoferrate (III). *Analytical and bioanalytical chemistry*. 2007 Jun;388:801-7.
- [6] Ghaedi M, Ahmadi F, Shokrollahi A. Simultaneous preconcentration and determination of copper, nickel, cobalt and lead ions content by flame atomic absorption spectrometry. *Journal of hazardous materials*. 2007 Apr 2;142(1-2):272-8.
- [7] Huang Y, Lin C, Luo F, Qiu B, Guo L, Lin Z, Chen G. Ultrasensitive and portable assay for lead (II) ions by electronic balance as a readout. *ACS sensors*. 2019 Sep 5;4(9):2465-70.
- [8] Jiang C, Li Y, Wang H, Chen D, Wen Y. A portable visual capillary sensor based on functional DNA crosslinked hydrogel for point-of-care detection of lead ion. *Sensors and Actuators B: Chemical*. 2020 Mar 15;307:127625.

- [9] Peng Z, Yu HR, Wen JY, Wang YL, Liang T, Cheng CJ. A novel ion-responsive photonic hydrogel sensor for portable visual detection and timely removal of lead ions in water. *Materials Advances*. 2022;3(13):5393-405.
- [10] Yap SH, Chien YH, Tan R, bin Shaik Alauddin AR, Ji WB, Tjin SC, Yong KT. An advanced hand-held microfiber-based sensor for ultrasensitive lead ion detection. *ACS sensors*. 2018 Nov 13;3(12):2506-12.
- [11] Yildirim N, Long F, He M, Gao C, Shi HC, Gu AZ. A portable DNAzyme-based optical biosensor for highly sensitive and selective detection of lead (II) in water sample. *Talanta*. 2014 Nov 1;129:617-22.
- [12] Zhou G, Chang J, Cui S, Pu H, Wen Z, Chen J. Real-time, selective detection of Pb<sup>2+</sup> in water using a reduced graphene oxide/gold nanoparticle field-effect transistor device. *ACS applied materials & interfaces*. 2014 Nov 12;6(21):19235-41.
- [13] Li Y, Wang C, Zhu Y, Zhou X, Xiang Y, He M, Zeng S. Fully integrated graphene electronic biosensor for label-free detection of lead (II) ion based on G-quadruplex structure-switching. *Biosensors and Bioelectronics*. 2017 Mar 15;89:758-63.
- [14] Maity A, Sui X, Tarman CR, Pu H, Chang J, Zhou G, Ren R, Mao S, Chen J. Pulse-driven capacitive lead ion detection with reduced graphene oxide field-effect transistor integrated with an analyzing device for rapid water quality monitoring. *ACS sensors*. 2017 Nov 22;2(11):1653-61.
- [15] Sui X, Pu H, Maity A, Chang J, Jin B, Lu G, Wang Y, Ren R, Mao S, Chen J. Field-effect transistor based on percolation network of reduced graphene oxide for real-time ppb-level detection of lead ions in water. *ECS Journal of Solid State Science and Technology*. 2020 Aug 10;9(11):115012.

1  
2  
3  
4  
5  
6  
7  
8  
9  
10  
11  
12  
13  
14  
15  
16  
17  
18  
19  
20  
21  
22  
23  
24  
25  
26  
27  
28  
29  
30  
31  
32  
33  
34  
35  
36  
37  
38  
39  
40  
41  
42  
43  
44  
45  
46  
47  
48  
49  
50  
51  
52  
53  
54  
55  
56  
57  
58  
59  
60

Downloaded on 29/12/2024 05:48:36  
This article is licensed under a Creative Commons Attribution 3.0 Unported Licence.



- 1  
2  
3 [16] Pullano SA, Critello CD, Mahbub I, Tasneem NT, Shamsir S, Islam SK, Greco M, Fiorillo  
4 AS. EGFET-based sensors for bioanalytical applications: A review. *Sensors*. 2018 Nov  
5 20;18(11):4042.  
6  
7  
8  
9  
10 [17] Kwon J, Lee BH, Kim SY, Park JY, Bae H, Choi YK, Ahn JH. Nanoscale FET-based  
11 transduction toward sensitive extended-gate biosensors. *ACS sensors*. 2019 Jun 4;4(6):1724-9.  
12  
13 [18] Jang HJ, Sui X, Zhuang W, Huang X, Chen M, Cai X, Wang Y, Ryu B, Pu H, Ankenbruck  
14 N, Beavis K. Remote floating-gate field-effect transistor with 2-dimensional reduced graphene  
15 oxide sensing layer for reliable detection of SARS-CoV-2 spike proteins. *ACS applied materials*  
16 & interfaces. 2022 May 20;14(21):24187-96.  
17  
18 [19] Jang HJ, Zhuang W, Sui X, Ryu B, Huang X, Chen M, Cai X, Pu H, Beavis K, Huang J, Chen  
19 J. Rapid, sensitive, label-free electrical detection of SARS-CoV-2 in nasal swab samples. *ACS*  
20 *applied materials & interfaces*. 2023 Mar 20;15(12):15195-202.  
21  
22 [20] Nag A, Mitra A, Mukhopadhyay SC. Graphene and its sensor-based applications: A review.  
23 *Sensors and Actuators A: physical*. 2018 Feb 1;270:177-94.  
24  
25 [21] Yavari F, Koratkar N. Graphene-based chemical sensors. *The journal of physical chemistry*  
26 *letters*. 2012 Jul 5;3(13):1746-53.  
27  
28 [22] Secor EB, Prabhumirashi PL, Puntambekar K, Geier ML, Hersam MC. Inkjet printing of high  
29 conductivity, flexible graphene patterns. *The journal of physical chemistry letters*. 2013 Apr  
30 18;4(8):1347-51.  
31  
32 [23] Gao Z, Wang L, Huang X, Benmore C, Pu H, Wen J, Zhuang W, Chan MK, Chen J. Selective  
33 single-atom adsorption for precision separation of lead ions in tap water via capacitive deionization.  
34 *Water Research*. 2025 Jan 1;268:122665.  
35  
36  
37  
38  
39  
40  
41  
42  
43  
44  
45  
46  
47  
48  
49  
50  
51  
52  
53  
54  
55  
56  
57  
58  
59  
60

- 1  
2  
3 [24] Wang C, Pu H, Sui X, Zhou S, Chen J. Hybrid modeling and sensitivity analysis on reduced  
4 graphene oxide field-effect transistor. *IEEE Transactions on Nanotechnology*. 2021 Apr  
5 27;20:404-16.  
6  
7  
8  
9  
10 [25] Kong N, Huang X, Cui L, Liu J. Surface modified graphene for heavy metal ions adsorption.  
11 *Science of Advanced Materials*. 2013 Aug 1;5(8):1083-9.  
12  
13 [26] Say R, Denizli A, Arica MY. Biosorption of cadmium (II), lead (II) and copper (II) with the  
14 filamentous fungus *Phanerochaete chrysosporium*. *Bioresource technology*. 2001 Jan 1;76(1):67-  
15 70.  
16  
17  
18 [27] Zhuang W, Jang HJ, Sui X, Ryu B, Wang Y, Pu H, Chen J. Enhancing Electrochemical  
19 Sensing through Molecular Engineering of Reduced Graphene Oxide–Solution Interfaces and  
20 Remote Floating-Gate FET Analysis. *ACS Applied Materials & Interfaces*. 2024 May 15.  
21  
22  
23 [28] Baachaoui S, Aldulaijan S, Sementa L, Fortunelli A, Dhouib A, Raouafi N. Density functional  
24 theory investigation of graphene functionalization with activated carbenes and its application in  
25 the sensing of heavy metallic cations. *The Journal of Physical Chemistry C*. 2021 Nov  
26 29;125(48):26418-28.  
27  
28  
29  
30  
31  
32  
33  
34  
35  
36  
37  
38  
39  
40  
41  
42  
43  
44  
45  
46  
47  
48  
49  
50  
51  
52  
53  
54  
55  
56  
57  
58  
59  
60

### Data Availability Statement

The authors declare that the data supporting the findings of this study are available in the paper and its Supplementary Information files. If raw data files in another format are needed, they can be obtained from the corresponding author upon reasonable request.

Environmental Science: Nano Accepted Manuscript

1  
2  
3  
4  
5  
6  
7  
8  
9  
10  
11  
12  
13  
14  
15  
16  
17  
18  
19  
20  
21  
22  
23  
24  
25  
26  
27  
28  
29  
30  
31  
32  
33  
34  
35  
36  
37  
38  
39  
40  
41  
42  
43  
44  
45  
46  
47  
48  
49  
50  
51  
52  
53  
54  
55  
56  
57  
58  
59  
60

Open Access Article. Published on 26 October 2024. Downloaded on 12/20/2024 4:05:48. This article is licensed under a Creative Commons Attribution 3.0 Unported Licence.

